Exceptional line and pseudospectrum in black hole spectroscopy

Li-Ming Cao, 1,2,* Ming-Fei Ji, 1,† Liang-Bi Wu, 3,4,‡ and Yu-Sen Zhou^{1,§}

¹Interdisciplinary Center for Theoretical Study and Department of Modern Physics,
University of Science and Technology of China, Hefei, Anhui 230026, China

²Peng Huanwu Center for Fundamental Theory, Hefei, Anhui 230026, China

³School of Fundamental Physics and Mathematical Sciences,
Hangzhou Institute for Advanced Study, UCAS, Hangzhou 310024, China

⁴University of Chinese Academy of Sciences, Beijing 100049, China
(Dated: November 24, 2025)

We investigate the exceptional points (EPs) and their pseudospectra in black hole perturbation theory. By considering a Gaussian bump modification to the Regge-Wheeler potential with variable amplitude, position, and width parameters, $(\varepsilon, d, \sigma_0)$, a continuous line of EPs (exceptional line, EL) in this three-dimensional parameter space is revealed. We find that the vorticity $\nu = \pm 1/2$ and the Berry phase $\gamma = \pi$ for loops encircling the EL, while $\nu = 0$ and $\gamma = 0$ for those do not encircle the EL. Through matrix perturbation theory, we prove that the ϵ -pseudospectrum contour size scales as $\epsilon^{1/q}$ at an EP, where q is the order of the largest Jordan block of the Hamiltonian-like operator, contrasting with the linear ϵ scaling at non-EPs. Numerical implements confirm this observation, demonstrating enhanced spectral instability at EPs for non-Hermitian systems including black holes.

I. INTRODUCTION

Upon characterizing the intrinsic oscillatory behavior of perturbed black holes (BHs), quasinormal modes (QNMs) manifest themselves as a discrete set of complex frequencies. The oscillation frequency is encoded in the real part, while the decay rate is encoded in the imaginary part. The QNMs not only act as spectral fingerprints that identify black holes, but also offer a powerful probe to test the Kerr hypothesis and explore gravity in the strong-field regime. This program is known as black hole spectroscopy [1–4].

Perturbed black holes are inherently non-Hermitian (NH) systems, a feature common across many branches of physics. Such NH systems offer fertile ground for exploring unique topological phenomena absent in Hermitian counterparts [5–8]. A defining hallmark of these systems is the appearance of the exceptional points (EPs) [9–14], where both eigenvalues and their corresponding eigenvectors coalesce. EPs naturally emerge in BH perturbation theory. Degenerate QNMs occur for massive scalar perturbations of Kerr black holes [15–17]. Similarly, EPs can be induced by adding a Gaussian bump to the original Regge-Wheeler (RW) effective potential [18]. Note that when there are insufficient free parameters, the phenomenon of EPs generally does not occur, and it is instead replaced by mode repulsion or avoided crossing [4, 19–23].

A remarkable property of EPs is their singular enhancement of sensitivity to parameter variations, an effect that surpasses anything possible in Hermitian systems [7]. This enhanced sensitivity has enabled diverse

applications, including advanced sensing platforms based on graphene metasurfaces and microtoroid cavities, integrated microresonators operating at three-fold EPs, coupled photonic cavities, and highly sensitive microcavity sensors for nanoparticle detection. Further applications span the detection of mechanical motion, electronics, and two-qubit systems, as detailed in [7].

To quantitatively study this enhanced sensitivity in black hole systems, pseudospectrum analysis provides an appropriate framework. Originally developed for nonselfadjoint operators, pseudospectrum analysis measures how eigenvalues respond to perturbations of norm ϵ [24]. Within the hyperboloidal framework, it has been employed to investigate QNM spectrum instability [24–28] for the gravity systems. The ϵ -pseudospectrum visually reveals stability through its contour structure in the complex plane, where open contours signify spectrum instability. This method has found broad application across diverse spacetimes [26, 29–49].

In this work, we first investigate the line of exceptional points in the 3-dimensional parameter space $(\varepsilon, d, \sigma_0)$ of the Gaussian bump-modified Regge-Wheeler potential. By varying the width parameter σ_0 , we find a continuous line of EPs, extending the single EP found in previous studies with fixed width. We then examine the topological properties of QNMs associated with this "exceptional line" (EL) by analyzing the winding of eigenvalues and the Berry phase along closed loops in parameter space. Finally, we study the pseudospectrum behavior at these EPs, both theoretically and numerically. Through matrix perturbation theory, we establish that the ϵ -pseudospectrum contour size scales as $\epsilon^{1/q}$ at an EP, where q is the order of the largest Jordan block, in contrast to the linear ϵ scaling away from EPs. This theoretical prediction is confirmed by numerical studies on the bump-modified Regge-Wheeler equation.

Supplemental materials include the hyperboloidal framework (Appendix A), a proof of Theorem 1 (Ap-

^{*} caolm@ustc.edu.cn

[†] jimingfei@mail.ustc.edu.cn

[‡] liangbi@mail.ustc.edu.cn

[§] zhou ys@mail.ustc.edu.cn

pendix B), a toy matrix model illustrating pseudospectrum behaviors at EPs (Appendix C), and an analysis of sample points of pseudospectra to demonstrate the scalings (Appendix D).

II. TOPOLOGICAL STRUCTURES OF QNMS ASSOCIATED WITH EXCEPTIONAL LINE

In [18], the authors investigate the QNM resonance arising from adding a Gaussian bump perturbation to the standard Regge-Wheeler potential governing axial (i.e., odd parity) perturbations of the Schwarzschild black hole. Therein, the bump depends on two parameters: the amplitude ε and the position d. They have found an EP at $\varepsilon=10^{-2.294}\simeq 0.005$ and d=15.698. Now, we further consider a Gaussian bump with changeable width. To be exact, we consider a master perturbation equation in the time-domain

$$\label{eq:potential} \Big[-\frac{\partial^2}{\partial t^2} + \frac{\partial^2}{\partial r^2} - V(r) \Big] \Psi(t,r) = 0 \,, \tag{1}$$

where $r_{\star} = r + 2M \ln(r - 2M)$ is the tortoise coordinate and V(r) is the bump-modified Regge-Wheeler potential [50], namely $V(r) = V_{\text{RW}}(r) + V_{\text{bump}}(r)$ with

$$V_{\rm RW}(r) = \left(1 - \frac{2M}{r}\right) \left(\frac{\ell(\ell+1)}{r^2} - \frac{6M}{r^3}\right),$$
 (2)

$$V_{\text{bump}}(r_{\star}) = \varepsilon \exp\left[-\frac{(r_{\star} - d)^2}{2\sigma_0^2}\right],$$
 (3)

where ε , d and σ_0 refer to the amplitude, position and width of the bump, respectively. For convenience, we use $2\sigma_0^2$ as the parameter that characterizes the width in the followings.

Within the hyperboloidal framework [26, 45, 51, 52] detailed in Appendix A, the time-domain perturbation equation (1) can be recasted into $\partial_{\tau}U=LU$, and thus the QNM spectra are just the spectra of L/i. We identify the EP where the fundamental mode and first overtone coalesce, in good agreement with the special case $2\sigma_0^2=1$ considered in [18]. By varying $2\sigma_0^2$, we systematically identify EPs in each constant- $2\sigma_0^2$ plane. These EPs collectively form a continuous line (exceptional line, EL) in the 3D parameter space $(\varepsilon, d, 2\sigma_0^2)$, as shown in Fig. 1. This demonstrates that EPs exist across a broader range of parameter configurations than previously recognized.

Analysis of Fig. 1 reveals systematic trends: as the Gaussian bump width σ_0 increases, the amplitude ε decreases and the bump position moves closer to the event horizon. Along the EL, $2\sigma_0^2$ varies by 300% from 0.5 to 2, while ε changes by approximately 39% from 0.0066 to 0.0040, and d changes by only 1.3% from 15.78 to 15.57. The corresponding QNM spectra evolve from 0.3671 + 0.1161i to 0.3648 + 0.1172i, with real and imaginary parts varying by approximately 0.6% and 0.9%, respectively. This indicates that while ε and $2\sigma_0^2$ exhibit

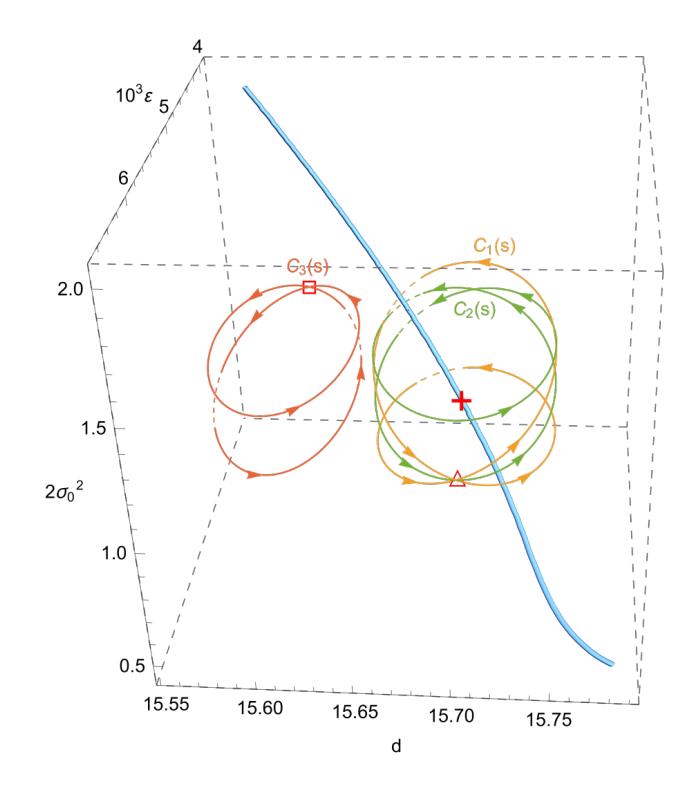


FIG. 1. The blue line is the EL in the 3D parameter space $(\varepsilon, d, 2\sigma_0^2)$. The symbol + marks the EP when $2\sigma_0^2 = 1$. The three closed curves $C_1(s)$ (yellow), $C_2(s)$ (green) and $C_3(s)$ (red). The \triangle is the point where $C_1(0)$ and $C_2(0)$ coincide, while the \square represents the point $C_3(0)$.

substantial variation along the EL, d and the corresponding QNM spectra remain relatively stable.

To investigate the topological structures of QNMs associated with this EL, we examine three closed curves $C_i(s)$, i = 1, 2, 3 in the 3D parameter space:

$$(b_{1i} + a_{1i}\cos(4\pi s), b_{2i} + a_{2i}\sin(4\pi s),$$

$$b_{3i} + a_{3i}\sin(2\pi s + \theta_i)), \quad s \in [0, 1],$$
 (4)

where a_{ji} , b_{ji} and θ_i are constant coefficients [53]. $C_1(s)$ and $C_2(s)$ encircle the EL twice, while $C_3(s)$ does not encircle it (see Fig. 1). All three curves exhibit counterclockwise rotation in the top view.

The two QNM spectra that coalesce at the EL is denoted as ω_+ and ω_- , and Fig. 2 displays the trajectories of them for each curves. All trajectories evolve clockwise. For $C_1(s)$, the two QNM spectra exchange positions as s increases from 0 to 0.5 and again from 0.5 to 1, returning to their initial positions at s=1. Similarly, for $C_2(s)$, exchange occurs between s=0.25 and s=0.75. In contrast, for $C_3(s)$, which does not encircle the EL, both $\omega_+(s)$ and $\omega_-(s)$ return to their initial positions without exchanging.

In non-Hermitian physics, the so-called vorticity can be introduced to describe the winding of each eigenvalues

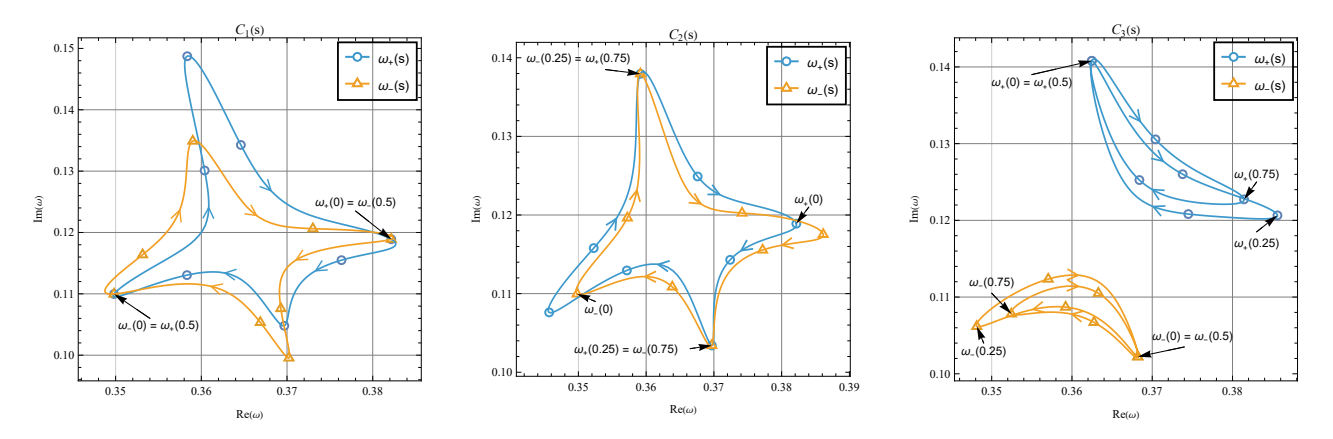


FIG. 2. Trajectories of $\omega_{+}(s)$ and $\omega_{-}(s)$ along the three parameter-space curves $C_1(s)$, $C_2(s)$, and $C_3(s)$. The positions of ω_{\pm} are explicitly marked by \circ and Δ , respectively, at discrete parameter values $s = 0, 0.125, 0.25, \dots, 1$.

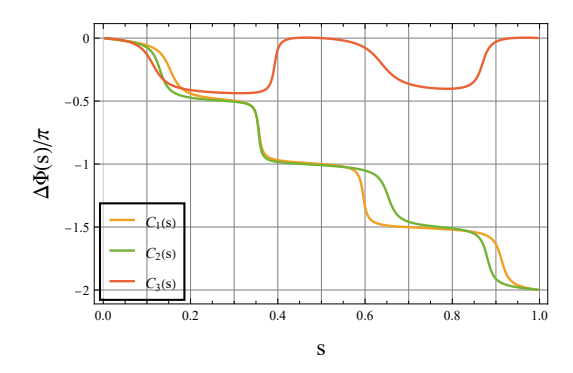


FIG. 3. $\Delta\Phi(s)$ for s varying from 0 to 1 for the three parameter-space curves $C_1(s), C_2(s)$, and $C_3(s)$.

around a single EP [54-56]. Its definition is

$$\nu(\Gamma) = -\frac{1}{2\pi} \oint_{\Gamma} d\Phi \,, \tag{5}$$

where $\Phi(s) = \arg\left(\omega_+(s) - \omega_-(s)\right)$, and Γ is a closed loop that encircles a single EP once. For a 2nd-order EP, the vorticity $\nu = \pm \frac{1}{2}$ [56]. To describe the winding of $\omega_+(s)$ and $\omega_-(s)$ in the complex plane, we plot the variation of $\Phi(s)$, i.e., $\Delta\Phi(s) = \Phi(s) - \Phi(0)$ for the three curves in Fig. 3. In our model, for a closed loop encircling the EL once, such as $s \in [0,0.5]$, $s \in [0.5,1]$ for C_1 or $s \in [0.25,0.75]$ for C_2 , each mode rotates π relative to the other and their trajectories forms a closed loop, hence $\Delta\Phi(s)$ changes $-\pi$ and $\nu = 1/2$. While, for a loop that do not encircle the EL like $s \in [0,0.5]$ or [0.5,1] for C_3 , the trajectory of each mode forms a closed loop and there are no change of $\Delta\Phi(s)$ in one period, hence $\nu = 0$.

Meanwhile, to study the phase evolution of these eigenvectors v_{\pm} under adiabatic variation of the parameter along a closed loop, we investigate the Berry phase in non-Hermitian system defined in [56–60]:

$$\gamma = i \oint_{C(s)} \frac{\langle u_i(s), \partial_s v_i(s) \rangle}{\langle u_i(s), v_i(s) \rangle} ds, \qquad (6)$$

where $i = \pm$ and u_{\pm} , v_{\pm} are left and right eigenvectors corresponding to ω_{\pm} respectively. The exact definitions of the left and right eigenvectors along with the inner product can be found in Appendix A. Note that there is a gauge freedom: we can multiply $v_i(s)$ by an arbitrary smooth function $\alpha(s)$ with $\alpha(0) = \alpha(1)$, resulting an ambiguity in γ , namely

$$\gamma \to \gamma' = \gamma + i \oint \frac{d\alpha}{\alpha} = \gamma + 2k\pi, \quad k \in \mathbb{Z},$$
 (7)

where k depends on the $\alpha(s)$ loop in the complex plane.

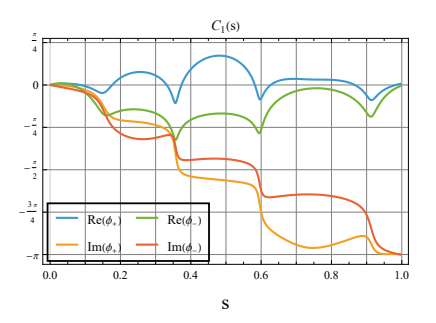
In practice, we use the spectral collocation method to obtain the finite-dimensional eigenvectors at each point of the parameter space. We fix the first element of the eigenvectors for gauge fixing by multiplying each eigenvector by a complex factor, which also ensures that the eigenvectors change continuously. The real and imaginary part of

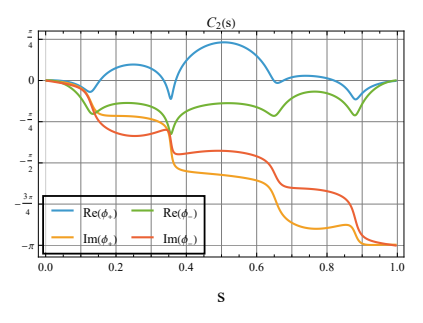
$$\phi_i(s) \equiv \int_0^s \frac{\langle u_i(s'), \partial_s v_i(s') \rangle}{\langle u_i(s'), v_i(s') \rangle} ds'$$
 (8)

for $s \in [0,1]$ are shown in Fig. 4. Note that $\operatorname{Im}(\phi_i(1)) = -\gamma$, while $\operatorname{Re}(\phi_i(1))$ vanishes theoretically. In Fig. 4, at s=1 the imaginary part is approximately $-\pi$ for C_1 and C_2 , and approximately 0 for C_3 at s=0.5, 1, while the real part vanishes in all cases. Thus, we confirm that the Berry phase is π for a curve that encircles the EL twice and 0 for a curve that do not encircle the EL, which is similar to the case of surrounding a single EP twice in a plane [61–65].

III. PSEUDOSPECTRUM AT EXCEPTIONAL POINTS

The existence of EPs raises an important question about their spectral stabilities, and how their spectral stabilities differ from that of the non-EPs. To address this, we employ pseudospectrum analysis, which provides





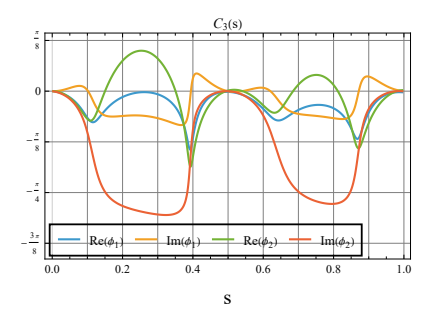


FIG. 4. The real and imaginary part of the integral (8) for the two near modes and the three curves, where the blue, orange, green and red lines denote $\text{Re}(\phi_+)$, $\text{Im}(\phi_+)$, $\text{Re}(\phi_-)$ and $\text{Im}(\phi_-)$ respectively.

a powerful framework for investigating spectrum instability for the non-Hermitian systems [24, 26, 27]. For an operator A and a given $\epsilon > 0$, the ϵ -pseudospectrum of the operator A is defined as

$$\sigma_{\epsilon}(A) = \{ z \in \mathbb{C} : \|(A - zI)^{-1}\| > \epsilon^{-1} \},$$
 (9)

where I denotes the identity operator. This definition proves most suitable for computational purposes. An equivalent yet more intuitive characterization is given by

$$\sigma_{\epsilon}(A) = \{ z \in \mathbb{C} : \exists \delta A, \text{ with } ||\delta A|| < \epsilon,$$
such that $z \in \sigma(A + \delta A) \},$ (10)

where $\sigma(A + \delta A)$ denotes the spectrum of $A + \delta A$. We also denote the boundary of $\sigma_{\epsilon}(A)$ as the ϵ -contour.

To elucidate the pseudospectra at EPs, we examine the perturbation theory for linear operators. Given an operator $A^{(0)}$, we introduce a family of perturbed operators $A(\varkappa)$ on $A^{(0)}$,

$$A(\varkappa) = A^{(0)} + \varkappa A^{(1)}, \qquad ||A^{(1)}|| < \infty.$$
 (11)

We concentrate on finite-dimensional matrices in the follows. The corresponding eigenvalue problem becomes

$$A(\varkappa)v_i(\varkappa) = \lambda_i(\varkappa)v_i(\varkappa). \tag{12}$$

For systems with simple eigenvalues λ_i , standard perturbation theory yields the expansions

$$\lambda_i(\varkappa) = \lambda_i^{(0)} + \varkappa \lambda_i^{(1)} + \mathcal{O}(\varkappa^2), \qquad (13)$$

$$v_i(\varkappa) = v_i^{(0)} + \varkappa v_i^{(1)} + \mathcal{O}(\varkappa^2).$$
 (14)

However, a parameter-dependent matrix is defective at its EP, and the conventional expansions (13) and (14) of eigenvalues and eigenvectors are no longer valid. For a EP located at $\varkappa = 0$, consider a circular loop in the complex \varkappa -plane centered at the EP, starting from a point \varkappa_0 . As \varkappa traverses this loop once, a continuous tracing of the eigenvalues $\lambda_i(\varkappa)$ results in a permutation of the initial eigenvalues, $\lambda_i(\varkappa_0)$. This permutation decomposes into disjoint cycles [66]:

$$\{\lambda_1, \lambda_2, \cdots, \lambda_{p_1}\}, \{\lambda_{p_1+1}, \lambda_{p_1+2}, \cdots, \lambda_{p_1+p_2}\}, \cdots, (15)$$

where each group undergoes a cyclic permutation after one encirclement in the \varkappa -plane. The number of elements p_i in each group is defined as the period of the corresponding cycle. The permutation depends on the specific form of $A^{(1)}$, and we denote the period of the largest possible cycle as q.

The eigenvalues that form a cycle of period p can be expanded as a Puiseux series. For $\varkappa \neq 0$, an eigenvalue $\lambda^{(0)}$ generally bifurcates into p distinct branches, i.e.,

$$\lambda_{h}(\varkappa) = \lambda^{(0)} + \lambda^{(1)} \left(e^{\frac{2\pi i(h-1)}{p}} \varkappa^{1/p} \right)^{1} + \lambda^{(2)} \left(e^{\frac{2\pi i(h-1)}{p}} \varkappa^{1/p} \right)^{2} + \mathcal{O}(\varkappa^{3/p}),$$

$$h = 1, 2, \dots, p,$$
(16)

which is also consistent with the cyclic permutation of period p. For small real \varkappa , the deviation $|\lambda_h(\varkappa) - \lambda^{(0)}| \propto \varkappa^{1/p}$ rather than $\propto \varkappa$, revealing the enhanced sensitivity of defective eigenvalues to perturbations compared to simple eigenvalues.

Given a small $\epsilon > 0$, consider the perturbation framework (11) with real $\varkappa \leqslant \epsilon$ and arbitrary $A^{(1)}$ with $||A^{(1)}|| = 1$, the original $\lambda^{(0)}$ bifurcates into λ_h . As indicated by (16), the deviation $\propto \varkappa^{1/p}$. Note that $\varkappa^{1/p}$ grows faster for larger p when $\varkappa \to 0$, thus the farthest possible deviation for all the $A^{(1)}$ is $\propto \epsilon^{1/q}$. On the other hand, in the context of pseudospectrum (10), an arbitrary perturbation δA can be identified as $\delta A = \|\delta A\| \frac{\delta A}{\|\delta A\|} \equiv \|\delta A\| A^{(1)} = \varkappa A^{(1)}$. This leads to the conclusion that the ϵ -contour, which marks the furthest deviation from the original eigenvalue, scales as $\propto \epsilon^{1/q}$. In case of a non-EP, where q = 1, we recover the ordinary linear ϵ scaling behavior. We have the following theorem for the relationship between the largest period and the Jordan blocks of the matrix $A^{(0)}$, which is proved in Appendix B.

Theorem 1. For a matrix perturbation problem $A(\varkappa) = A^{(0)} + \varkappa A^{(1)}$ with $||A^{(1)}|| < \infty$, a degenerate eigenvalue $\lambda_i^{(0)}$ of $A^{(0)}$ bifurcates into several groups of eigenvalue $\{\lambda_1, \lambda_2, \cdots, \lambda_{p_1}\}, \{\lambda_{p_1+1}, \lambda_{p_1+2}, \cdots, \lambda_{p_1+p_2}\}, \cdots$, where each group undergoes a cyclic permutation when \varkappa goes around 0 in the complex plane. The largest possible period q (or the largest possible number of the eigenvalues

in a cycle) for all $A^{(1)}$ is just the index of the eigenvalue $\lambda_i^{(0)}$, i.e., the order of the largest Jordan block of the eigenvalue.

The following conclusions can be drawn from the above discussions: the ϵ -contours of a matrix $A^{(0)}$ near a certain eigenvalue $\lambda^{(0)}$ scales as $\epsilon^{1/q}$ when $\epsilon \to 0$ with q is the order of the largest Jordan block of this eigenvalue. A toy model is provided in Appendix C to illustrate this statement.

We now proceed to the computation of the black hole's pseudospectrum $\sigma_{\epsilon}(L/\mathrm{i})$ (see Appendix A for the construction of L), noting that the choice of the norm significantly influences pseudospectrum's shape and structure. Fig. 5 displays pseudospectra near the fundamental mode at $\varepsilon=0.005,\ d=15,\ 2\sigma_0^2=1$ (non-EP case) and at the exceptional point $\varepsilon=0.005083,\ d=15.6976,\ 2\sigma_0^2=1$ (EP case). Our analysis reveals that inscribed circles with radii proportional to ϵ provide superior fitting for non-EP configurations, while radii scaling as $\epsilon^{1/2}$ better characterize EP cases, consistent with the above theoretical predictions.

To further validate the scaling behavior of ϵ -pseudospectrum contours, we analyze horizontal and vertical cross sections through the pseudospectrum structure (see Appendix D). These cross-sectional analyses provide additional evidence for the characteristic $\epsilon^{1/2}$ scaling at EPs compared to the linear ϵ scaling away from EPs, reinforcing our theoretical predictions with comprehensive numerical verification.

The enhanced QNM spectra instability at EPs manifests clearly in the pseudospectrum structure. For sufficiently small ϵ , the $\epsilon^{1/2}$ scaling demonstrates remarkably faster variation compared to linear ϵ scaling, indicating enhanced QNM spectrum instability when deviating from EPs in parameter space. The physical implications of these findings extend to gravitational wave physics and black hole spectroscopy. The $e^{1/2}$ scaling at second-order EPs implies that small perturbations could induce disproportionately large shifts in QNM spectra near EPs. The spectrum instability near EPs necessitates careful assessment of ringdown model reliability in gravitational wave analysis, as small systematic errors could be amplified in EP regions. Our results establish a framework for evaluating such spectrum stability across the black hole parameter space, with particular relevance for future high-precision gravitational wave observations.

IV. CONCLUSIONS AND DISCUSSION

We find a continuous line of EPs (exceptional line. EL) in the 3D parameter space $(\varepsilon, d, \sigma_0)$ of the Gaussian bump-modified Regge-Wheeler potential. This EL exhibits rich topological characteristics: loops encircling the EL acquire the vorticity $\nu = \pm 1/2$ and the Berry phase $\gamma = \pi$, while loops not encircling the EL yield $\nu = 0$ and $\gamma = 0$. Next, through matrix perturbation theory, we find that the ϵ -pseudospectrum contour size scales as $\epsilon^{1/q}$ at an EP, where q is the order of the largest Jordan block of the corresponding degenerate eigenvalue, in contrast to the linear ϵ scaling at non-EPs. Numerical computations at a second-order EP in the EL provide strong confirmation of this theoretical prediction, demonstrating $e^{1/2}$ scaling at second-order EPs compared to linear ϵ scaling away from EPs, which highlights the enhanced spectrum instability characteristic of non-Hermitian systems.

Looking forward, our work opens several promising research directions. The theoretical framework developed for matrix perturbation problems near EPs, particularly Theorem 1, can be generalized to study eigenvalue sensitivity enhancement in non-Hermitian systems across various physical domains beyond black hole physics. Moreover, as the first application of pseudospectrum methods to investigate QNM spectrum stability near EPs in gravitational contexts, our approach provides a universal methodology that can be extended to study spectrum stability around EPs in other physical systems. Beyond the current context, similar EP phenomena may exist in perturbations of rotating black holes [15–17], wormholes, and exotic compact objects [67]. Although EPs constitute measure-zero points in parameter space, they can exert strong effects on parameter regions surrounding the EP. The topological properties of these regions, including mode exchange when encircling EPs and the corresponding vorticity and Berry phase phenomena, warrant detailed investigation. Importantly, for gravitational wave observations, the heightened QNM spectral instability near EPs necessitates developing new waveform templates that account for this enhanced sensitivity, such as those proposed in [18], potentially improving the accuracy of black hole spectroscopy in future gravitational wave detectors. Regarding QNM spectroscopy, our work demonstrates the necessity of applying Puiseux series similar to Eq. (16) near EPs in the parameterized analysis of QNMs.

ACKNOWLEDGEMENT

This work is supported in part by the National Key R&D Program of China Grant No. 2022YFC2204603, by the National Natural Science Foundation of China with grants No.12475063, No. 12075232, No. 12247103. and No. 12505067.

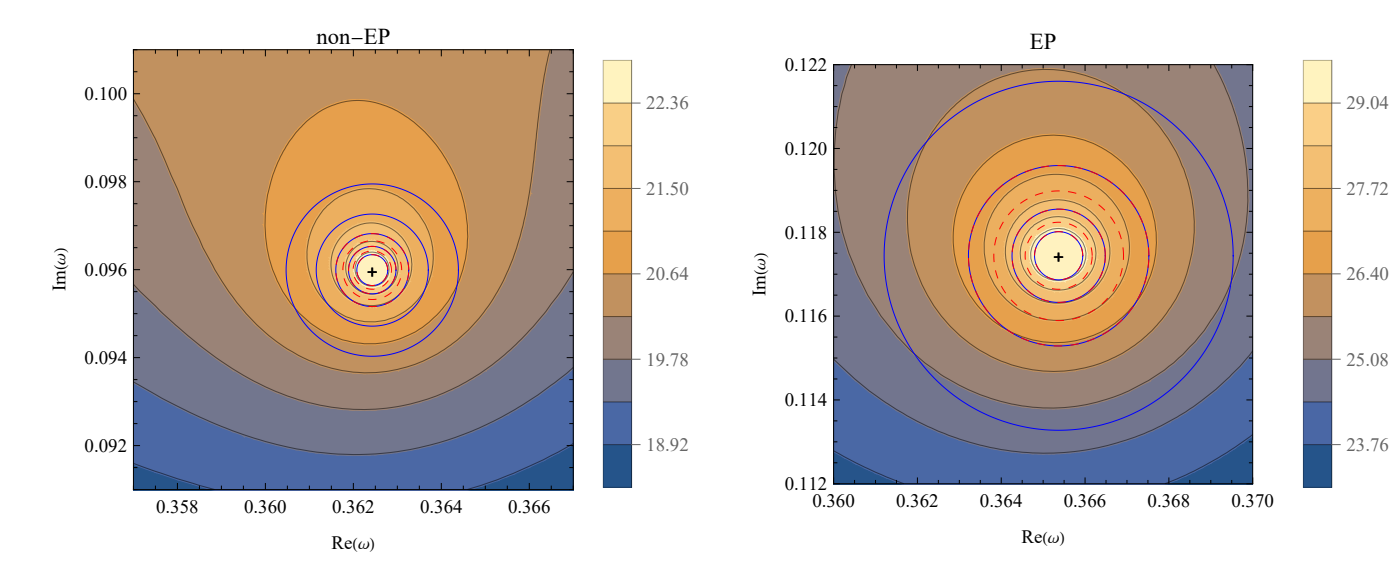


FIG. 5. Pseudospectrum of Regge-Wheeler potential with a bump modification near the fundamental mode at non-EP $\varepsilon = 0.005$, $d = 15, 2\sigma_0^2 = 1$ (left panel) and at the EP $\varepsilon = 0.005083$, $d = 15.6976, 2\sigma_0^2 = 1$ (right panel) by plotting $-\ln(\epsilon)$. We fit the smallest circle inscribed in the innermost contour, the red dashed lines and the blue lines are a group of circles centered in the QNM spectrum, and their radius are proportional to $\epsilon^{1/2}$ and ϵ respectively.

- [1] K. D. Kokkotas and B. G. Schmidt, Living Rev. Rel. 2, 2 (1999), arXiv:gr-qc/9909058.
- [2] E. Berti, V. Cardoso, and A. O. Starinets, Class. Quant. Grav. 26, 163001 (2009), arXiv:0905.2975 [gr-qc].
- [3] R. A. Konoplya and A. Zhidenko, Rev. Mod. Phys. 83, 793 (2011), arXiv:1102.4014 [gr-qc].
- [4] E. Berti et al., (2025), arXiv:2505.23895 [gr-qc].
- [5] N. Moiseyev, Non-Hermitian Quantum Mechanics (Cambridge University Press, 2011).
- [6] R. El-Ganainy, K. G. Makris, M. Khajavikhan, Z. H. Musslimani, S. Rotter, and D. N. Christodoulides, Nature Phys. 14, 11 (2018).
- [7] Y. Ashida, Z. Gong, and M. Ueda, Adv. Phys. 69, 249 (2021), arXiv:2006.01837 [cond-mat.mes-hall].
- [8] E. J. Bergholtz, J. C. Budich, and F. K. Kunst, Rev. Mod. Phys. 93, 015005 (2021), arXiv:1912.10048 [cond-mat.mes-hall].
- [9] W. D. Heiss and A. L. Sannino, 23, 1167 (1990).
- [10] J.-W. Ryu, S.-Y. Lee, and S. W. Kim, Physical Review A 79 (2009), 10.1103/physreva.79.053858.
- [11] B. Dietz, H. L. Harney, O. N. Kirillov, M. Miski-Oglu, A. Richter, and F. Schaefer, Phys. Rev. Lett. 106, 150403 (2011), arXiv:1008.2623 [nlin.CD].
- [12] H. Xu, D. Mason, L. Jiang, and J. G. E. Harris, Nature 537, 80 (2016), arXiv:1602.06881 [physics.optics].
- [13] P. Miao, Z. Zhang, J. Sun, W. Walasik, S. Longhi, N. M. Litchinitser, and L. Feng, Science 353, 464 (2016), https://www.science.org/doi/pdf/10.1126/science.aaf8533.
- [14] K. Ding, G. Ma, M. Xiao, Z. Zhang, and C. Chan, Physical Review X 6 (2016), 10.1103/physrevx.6.021007.
- [15] J. P. Cavalcante, M. Richartz, and B. C. da Cunha, Phys. Rev. Lett. 133, 261401 (2024), arXiv:2407.20850 [gr-qc].
- [16] J. P. Cavalcante, M. Richartz, and B. C. da Cunha, Phys. Rev. D 110, 124064 (2024), arXiv:2408.13964 [gr-qc].

- [17] J. P. Cavalcante, M. Richartz, and B. C. da Cunha, (2025), arXiv:2511.16640 [gr-qc].
- [18] Y. Yang, E. Berti, and N. Franchini, Phys. Rev. Lett. 135, 201401 (2025), arXiv:2504.06072 [gr-qc].
- [19] O. J. C. Dias, M. Godazgar, J. E. Santos, G. Carullo, W. Del Pozzo, and D. Laghi, Phys. Rev. D 105, 084044 (2022), arXiv:2109.13949 [gr-qc].
- [20] H. Motohashi, Phys. Rev. Lett. 134, 141401 (2025), arXiv:2407.15191 [gr-qc].
- [21] N. Oshita, E. Berti, and V. Cardoso, Phys. Rev. Lett. 135, 031401 (2025), arXiv:2503.21276 [gr-qc].
- [22] R. K. L. Lo, L. Sabani, and V. Cardoso, Phys. Rev. D 111, 124002 (2025), arXiv:2504.00084 [gr-qc].
- [23] T. Takahashi, H. Motohashi, and K. Takahashi, Phys. Rev. D 112, 064006 (2025), arXiv:2505.03883 [gr-qc].
- [24] L. Trefethen and M. Embree, Spectra and Pseudospectra: The Behavior of Nonnormal Matrices and Operators (Princeton university press, 2005).
- [25] V. Boyanov, Front. in Phys. 12, 1511757 (2024), arXiv:2410.11547 [gr-qc].
- [26] J. L. Jaramillo, R. Panosso Macedo, and L. Al Sheikh, Phys. Rev. X 11, 031003 (2021), arXiv:2004.06434 [gr-qc].
- [27] K. Destounis and F. Duque (2023) arXiv:2308.16227 [gr-qc].
- [28] J. L. Jaramillo, R. Panosso Macedo, and L. A. Sheikh, Phys. Rev. Lett. 128, 211102 (2022), arXiv:2105.03451 [gr-qc].
- [29] K. Destounis, R. P. Macedo, E. Berti, V. Cardoso, and J. L. Jaramillo, Phys. Rev. D 104, 084091 (2021), arXiv:2107.09673 [gr-qc].
- [30] L.-M. Cao, J.-N. Chen, L.-B. Wu, L. Xie, and Y.-S. Zhou, Sci. China Phys. Mech. Astron. 67, 100412 (2024), arXiv:2401.09907 [gr-qc].

- [31] S. Sarkar, M. Rahman, and S. Chakraborty, Phys. Rev. D 108, 104002 (2023), arXiv:2304.06829 [gr-qc].
- [32] K. Destounis, V. Boyanov, and R. Panosso Macedo, Phys. Rev. D 109, 044023 (2024), arXiv:2312.11630 [gr-qc].
- [33] S. Luo, Phys. Rev. D 110, 084071 (2024), arXiv:2408.08139 [gr-qc].
- [34] C. Warnick, (2024), arXiv:2407.19850 [gr-qc].
- [35] D. Arean, D. Garcia-Fariña, and K. Landsteiner, Front. in Phys. 12, 1460268 (2024), arXiv:2407.04372 [hep-th].
- [36] B. Cownden, C. Pantelidou, and M. Zilhão, JHEP 05, 202 (2024), arXiv:2312.08352 [gr-qc].
- [37] V. Boyanov, V. Cardoso, K. Destounis, J. L. Jaramillo, and R. Panosso Macedo, Phys. Rev. D 109, 064068 (2024), arXiv:2312.11998 [gr-qc].
- [38] D. Garcia-Fariña, K. Landsteiner, P. G. Romeu, and P. Saura-Bastida, JHEP 01, 185 (2025), arXiv:2407.06104 [hep-th].
- [39] D. Areán, D. G. Fariña, and K. Landsteiner, JHEP 12, 187 (2023), arXiv:2307.08751 [hep-th].
- [40] V. Boyanov, K. Destounis, R. Panosso Macedo, V. Cardoso, and J. L. Jaramillo, Phys. Rev. D 107, 064012 (2023), arXiv:2209.12950 [gr-qc].
- [41] L.-M. Cao, L.-B. Wu, and Y.-S. Zhou, Sci. China Phys. Mech. Astron. 68, 100411 (2025), arXiv:2412.21092 [gr-qc].
- [42] J. Carballo, C. Pantelidou, and B. Withers, (2025), arXiv:2503.05871 [gr-qc].
- [43] J.-N. Chen, L.-B. Wu, and Z.-K. Guo, Class. Quant. Grav. 41, 235015 (2024), arXiv:2407.03907 [gr-qc].
- [44] P. H. C. Siqueira, L. T. de Paula, R. Panosso Macedo, and M. Richartz, Phys. Rev. D 111, 104039 (2025), arXiv:2501.13815 [gr-qc].
- [45] J. Besson and J. L. Jaramillo, (2024), arXiv:2412.02793 [gr-qc].
- [46] L. T. de Paula, P. H. C. Siqueira, R. Panosso Macedo, and M. Richartz, Phys. Rev. D 111, 104064 (2025), arXiv:2504.00106 [gr-qc].
- [47] R.-G. Cai, L.-M. Cao, J.-N. Chen, Z.-K. Guo, L.-B. Wu, and Y.-S. Zhou, Phys. Rev. D 111, 084011 (2025), arXiv:2501.02522 [gr-qc].
- [48] J. Carballo and B. Withers, JHEP 10, 084 (2024), arXiv:2406.06685 [hep-th].
- [49] L.-M. Cao, M.-F. Ji, L.-B. Wu, and Y.-S. Zhou, (2025), arXiv:2508.13894 [gr-qc].
- [50] M. H.-Y. Cheung, K. Destounis, R. P. Macedo, E. Berti, and V. Cardoso, Phys. Rev. Lett. 128, 111103 (2022), arXiv:2111.05415 [gr-qc].
- [51] R. Panosso Macedo, Phil. Trans. Roy. Soc. Lond. A 382, 20230046 (2024), arXiv:2307.15735 [gr-qc].
- [52] E. Gasperin and J. L. Jaramillo, Class. Quant. Grav. 39, 115010 (2022), arXiv:2107.12865 [gr-qc].
- [53] These coefficients are explicitly given by: $b_{11} = 0.005\,, \quad a_{11} = 0.001\,, \quad b_{21} = 15.7\,, \\ a_{21} = 0.05\,, \quad b_{31} = 1\,, \qquad a_{31} = 0.25\,, \quad \theta_1 = 0\,; \\ b_{12} = 0.005\,, \quad a_{12} = 0.001\,, \quad b_{22} = 15.7\,, \\ a_{22} = 0.05\,, \quad b_{32} = 1.125\,, \quad a_{32} = 0.125\,, \quad \theta_2 = -\pi/2\,; \\ b_{13} = 0.005\,, \quad a_{13} = -0.001\,, \quad b_{23} = 15.6\,, \\ a_{23} = -0.04\,, \quad b_{33} = 1.125\,, \quad a_{33} = 0.125\,, \quad \theta_3 = 0\,.$
- [54] D. Leykam, K. Y. Bliokh, C. Huang, Y. D. Chong, and F. Nori, Phys. Rev. Lett. 118, 040401 (2017), arXiv:1610.04029 [cond-mat.mes-hall].
- [55] H. Shen, B. Zhen, and L. Fu, Physical Review Letters 120 (2018), 10.1103/physrevlett.120.146402.

- [56] J.-W. Ryu, J.-H. Han, and C.-H. Yi, (2025), arXiv:2509.09129 [physics.optics].
- [57] J. Garrison and E. Wright, Physics Letters A 128, 177 (1988).
- [58] G. Dattoli, R. Mignani, and A. Torre, Journal of Physics A: Mathematical and General 23, 5795 (1990).
- [59] A. Mostafazadeh, Phys. Lett. A 264, 11 (1999), arXiv:quant-ph/9911003.
- [60] S.-D. Liang and G.-Y. Huang, (2015), 10.1103/Phys-RevA.87.012118, arXiv:1502.00443 [quant-ph].
- [61] W. D. Heiss, J. Phys. A 45, 444016 (2012), arXiv:1210.7536 [quant-ph].
- [62] T. Gao et al., Nature 526, 554 (2015), arXiv:1504.00978 [cond-mat.quant-gas].
- [63] C. Dembowski, B. Dietz, H.-D. Gräf, H. L. Harney, A. Heine, W. D. Heiss, and A. Richter, Phys. Rev. E 69, 056216 (2004).
- [64] R. Lefebvre, O. Atabek, M. Šindelka, and N. Moiseyev, Phys. Rev. Lett. 103, 123003 (2009).
- [65] A. A. Mailybaev, O. N. Kirillov, and A. P. Seyranian, Phys. Rev. A 72, 014104 (2005), arXiv:quant-ph/0501040.
- [66] T. Kato, Perturbation Theory for Linear Operators, Classics in mathematics (Springer Berlin Heidelberg, 1976).
- [67] L.-B. Wu, L. Xie, M.-F. Ji, Y.-S. Zhou and L.-M. Cao work in progress.

SUPPLEMENT MATERIAL

Appendix A: The hyperboloidal framework

The compact hyperboloidal coordinates $(\tau, \sigma, \theta, \varphi)$ related with original coordinate (t, r, θ, φ) are defined as follows

$$t = \tau - h(\sigma),$$

 $r = \frac{r_{\rm h}}{\sigma},$ (A1)

where $h(\sigma)$ is the height function. The coordinate σ spans the interval [0,1], with $\sigma=0$ corresponding to null infinity \mathscr{I}^+ and $\sigma=1$ to the event horizon \mathscr{H}^+ . Following the approach in [51], we adopt the height function

$$h(\sigma) = 2M \left[-\frac{1}{\sigma} + \ln \sigma + \ln(1 - \sigma) \right], \quad (A2)$$

and set M=1 for the unit.

In these coordinates, the master perturbation equation (1) transforms to

$$\partial_{\tau}U = LU$$
, $L = \begin{pmatrix} 0 & 1 \\ L_1 & L_2 \end{pmatrix}$, $U = \begin{pmatrix} \Psi \\ \Pi \end{pmatrix}$, (A3)

with $\Pi \equiv \partial_{\tau} \Psi$. The differential operators L_1 and L_2 are given by

$$L_1 = \frac{1}{w(\sigma)} \left[\partial_{\sigma}(p(\sigma)\partial_{\sigma}) - q(\sigma) \right], \quad (A4)$$

$$L_2 = \frac{1}{w(\sigma)} \Big[2\gamma(\sigma)\partial_{\sigma} + \partial_{\sigma}\gamma(\sigma) \Big], \qquad (A5)$$

where above functions read

$$p(\sigma) = \frac{\sigma^2 f(r(\sigma))}{r_{\rm h}}, \quad \gamma(\sigma) = h'(\sigma) p(\sigma),$$

$$w(\sigma) = \frac{1 - \gamma^2(\sigma)}{p(\sigma)}, \quad q(\sigma) = \frac{V(\sigma)}{p(\sigma)}. \tag{A6}$$

Here the prime denotes differentiation with respect to σ . Consider the Fourier transform of $U(\tau, \sigma)$ with respect to time τ , we have

$$U(\tau, \sigma) = e^{i\omega t} \tilde{U}(r_{\star}) = e^{i\omega \tau} U(\sigma), \qquad (A7)$$

where $U(\sigma) = e^{-i\omega h(\sigma)}\tilde{U}(r_{\star})$ from Eqs. (A1). Then the problem of solving QNM spectra turns into an eigenvalue problem $LU = i\omega U$. In practice, we apply the spectral collocation method and discretize σ in Chebyshev-Lobatto grid with N = 300.

To support the concepts appeared in this work, including the vorticity, the Berry phase, the Petermann factors and the pseudospectrum of EPs, we give an introduction to the left and right eigenvectors along with the inner product and the norm. Consider a linear operator A acting on a complex vector space equipped with inner product $\langle \cdot, \cdot \rangle$, and denote its adjoint as A^{\dagger} , defined through

 $\langle A^{\dagger}u, v \rangle = \langle u, Av \rangle$. The left u_i and right v_i eigenvectors satisfy respectively

$$A^{\dagger}u_i = \bar{\lambda}_i u_i \,, \quad Av_i = \lambda_i v_i \,, \tag{A8}$$

where $\bar{\lambda}_i$ is the complex conjugate of λ_i . We adopt the energy inner product

$$\langle U_1, U_2 \rangle_{\mathcal{E}} = \left\langle \begin{pmatrix} \Psi_1 \\ \Pi_1 \end{pmatrix}, \begin{pmatrix} \Psi_2 \\ \Pi_2 \end{pmatrix} \right\rangle_{\mathcal{E}}$$

$$= \frac{1}{2} \int_0^1 \left(w(\sigma) \bar{\Pi}_1 \Pi_2 + p(\sigma) \partial_\sigma \bar{\Psi}_1 \partial_\sigma \Psi_2 + q(\sigma) \bar{\Psi}_1 \Psi_2 \right) d\sigma ,$$
(A9)

where a bar represents the complex conjugate, and three functions $w(\sigma)$, $p(\sigma)$, $q(\sigma)$ are given by Eqs. (A6). Therefore, a physically meaningful norm for the function $U(\sigma)$, namely the energy norm [26, 45, 52], can be induced as

$$||U||_{\mathcal{E}} = \sqrt{\langle U, U \rangle_{\mathcal{E}}},$$
 (A10)

which is chosen to implement the pseudospectrum.

Solving the eigenvalue problem, we identify EPs where the fundamental mode coincides with the first overtone and their eigenvectors coalesce. The model in [18] corresponds to the special case $2\sigma_0^2=1$, and for this case, we find an EP at $\varepsilon=0.005083$, d=15.6976 with nearly coincident spectra $\omega_+=0.36520+0.11743$ i and $\omega_-=0.36554+0.11745$ i. Their eigenvectors also demonstrate near-perfect coalescence, confirming such parameter as a genuine EP. The phase rigidity r_i and Petermann factor K_i are defined as

$$r_i = \frac{|\langle u_i, v_i \rangle|}{\sqrt{\langle u_i, u_i \rangle \langle v_i, v_i \rangle}} \equiv \frac{1}{\kappa_i}, \quad K_i = \frac{1}{r_i^2} \equiv \kappa_i^2, \text{ (A11)}$$

where u_i and v_i are left and right eigenvectors defined in Eqs. (A8). In Eqs. (A11), κ_i is the condition number, and the subscript i refers to the index of eigenvalues. For normal operators, $\kappa_i = K_i = r_i = 1$, whereas for nonnormal operators $\kappa_i > 1$, $K_i > 1$, and $r_i < 1$. Using the energy norm defined in Eq. (A10), it can be found that $r_+ \simeq 2.03 \times 10^{-10}$, $r_- \simeq 2.04 \times 10^{-10}$ and $K_+ \simeq 2.43 \times 10^{19}$, $K_- \simeq 2.40 \times 10^{19}$, indicating extreme nonnormality around aforementioned EP.

Appendix B: Proof of the Theorem 1

We first prove, for small real \varkappa , that the largest possible value of p in the expansion given by Eq. (16) is equal to the index of the eigenvalue. Then, the equivalence between the period of the largest permutation cycle and the largest possible value of p can be derived through complex analytical continuation from the expansion of real \varkappa in Eq. (16).

Consider a matrix $A(\varkappa) = A^{(0)} + \varkappa A^{(1)}$ and $A^{(1)}$ is bounded, we consider an eigenvalue $\lambda(\varkappa)$ and one of its

eigenvectors $v(\varkappa)$ whose expansion are the same as (13) and (14) respectively but the subscript i is ignored. To begin with, the definition of root subspace or generalized eigenspace of a $n \times n$ matrix A and its eigenvalue λ is

$$\mathcal{R}_{\lambda}(A) := \{ v \in \mathbb{C}^n | \exists k \in \mathbb{N}, (A - \lambda I)^k v = 0 \}.$$
 (B1)

The smallest positive integer ν that satisfies

$$(A^{(0)} - \lambda^{(0)}I)^{\nu}u = 0, \forall u \in \mathcal{R}_{\lambda^{(0)}}(A^{(0)}),$$
 (B2)

from which ν is called the index of the eigenvalue $\lambda^{(0)}$, which is just the order of the largest Jordan block of it. We note that for every integer k larger than the index, $(A^{(0)} - \lambda^{(0)}I)^k u = 0$, $\forall u \in \mathcal{R}_{\lambda^{(0)}}(A)$. Noticing this identity for polynomials

$$X^{\nu} - Y^{\nu} = (X - Y)(X^{\nu - 1} + X^{\nu - 2}Y + \dots + Y^{\nu - 1}),$$
(B3)

for commutable matrices $A(\varkappa) - \lambda^{(0)}I$ and $(\lambda(\varkappa) - \lambda^{(0)})I$, we can obtain

$$(A(\varkappa) - \lambda^{(0)}I)^{\nu} - (\lambda(\varkappa) - \lambda^{(0)})^{\nu}I$$

= $(A(\varkappa) - \lambda(\varkappa)I) \cdot Q(A(\varkappa), \lambda(\varkappa)),$ (B4)

where $Q(A(\varkappa), \lambda(\varkappa))$ is a polynomial matrix of $A(\varkappa)$ and $\lambda(\varkappa)$ of order $\nu - 1$.

The eigenvector $v(\varkappa)$ corresponding to $\lambda(\varkappa)$ satisfies

$$(A(\varkappa) - \lambda(\varkappa)I)v(\varkappa) = 0.$$
 (B5)

multiplying both side of the Eq. (B4) to $v(\varkappa)$, and we can find that the right hand side vanishes, thus

$$(A^{(0)} + \varkappa A^{(1)} - \lambda^{(0)} I)^{\nu} v(\varkappa) = (\lambda(\varkappa) - \lambda^{(0)})^{\nu} v(\varkappa) \text{ (B6)}$$

We expand the left hand side as Taylor series of \varkappa . As $v^{(0)} \in \mathcal{R}_{\lambda^{(0)}}(A^{(0)})$, the $\mathcal{O}(\varkappa^0)$ term $(A^{(0)} - \lambda^{(0)}I)^{\nu}v^{(0)} = 0$, therefore

$$C_1 \varkappa v^{(0)} + C_2 \varkappa v^{(1)} + \mathcal{O}(\varkappa^2) = (\lambda(\varkappa) - \lambda^{(0)})^{\nu} v(\varkappa)$$
,(B7)

in which C_1 and C_2 are bounded constant matrices. Taking the norm of the above equation and we can obtain

$$|\lambda(\varkappa) - \lambda^{(0)}|^{\nu} ||v(\varkappa)||$$

$$= ||C_1 \varkappa v^{(0)} + C_2 \varkappa v^{(1)} + \mathcal{O}(\varkappa^2)||$$

$$\leq (||C_1 v^{(0)}|| + ||C_2 v^{(1)}||) \varkappa + \mathcal{O}(\varkappa^2), \quad (B8)$$

where we set $\varkappa > 0$ for simplicity. Divide both sides of (B8) by $||v(\varkappa)||$, hence

$$|\lambda(\varkappa) - \lambda^{(0)}|^{\nu} \leqslant \frac{\|C_1 v^{(0)}\| + \|C_2 v^{(1)}\|}{\|v(\varkappa)\|} \varkappa + \mathcal{O}(\varkappa^2)$$

$$= \frac{\|C_1 v^{(0)}\| + \|C_2 v^{(1)}\|}{\|v^{(0)}\|} \varkappa + \mathcal{O}(\varkappa^2).$$
(B9)

Thus, for a small enough \varkappa , there exist a constant K > 0 and

$$|\lambda(\varkappa) - \lambda^{(0)}|^{\nu} \leqslant K\varkappa, \tag{B10}$$

or equivalently

$$|\lambda(\varkappa) - \lambda^{(0)}| \leqslant K^{1/\nu} \varkappa^{1/\nu} . \tag{B11}$$

This indicates that the largest possible p in the expansion Eq. (16) is no greater than the index ν . Moreover, there exists a kind of perturbation such that p saturates the upper bound ν . Consider the Jordan decomposition of the matrix $A^{(0)}$, which contains a $\nu \times \nu$ Jordan block of eigenvalue $\lambda^{(0)}$

$$J_{\nu} = \begin{pmatrix} \lambda^{(0)} & 1 & & 0 \\ & \lambda^{(0)} & \ddots & & \\ & & \ddots & \ddots & \\ & & & \lambda^{(0)} & 1 \\ 0 & & & \lambda^{(0)} \end{pmatrix}, \tag{B12}$$

we can choose the perturbation matrix such that it perturbs J_{ν} as

$$\varkappa \delta J_{\nu} = \begin{pmatrix} 0 & 0 & \cdots & 0 \\ \vdots & \vdots & & \vdots \\ 0 & 0 & \cdots & 0 \\ \varkappa & 0 & \cdots & 0 \end{pmatrix} , \tag{B13}$$

then the eigenvalues of $J_{\nu}(\lambda) + \varkappa \delta J_{\nu}(\lambda)$ are $\lambda_h = \lambda^{(0)} + \varkappa^{1/\nu} \exp\left(\frac{2\pi \mathrm{i}(h-1)}{\nu}\right)$ with $h = 1, 2, \dots, \nu$. After the complex analytical continuation on \varkappa they are all in one cycle with period ν .

Therefore, we have proved that for a fixed $A^{(0)}$ the largest period of eigenvalue $\lambda_i(\varkappa)$ for $A(\varkappa) = A^{(0)} + \varkappa A^{(1)}$ for all possible $A^{(1)}$ is the index of the eigenvalue λ_i of $A^{(0)}$.

Appendix C: A toy model

In this appendix, in order to show the essential differences of the pseudospectra between the non-EP and the EP. We focus on a toy model, namely a two-dimensional non-normal matrix (unless x=1) given by

$$\mathbf{A}(x) = \begin{pmatrix} x & 1 \\ x & -x \end{pmatrix} \,, \tag{C1}$$

where $x \in \mathbb{C}$ refers to the parameter of \mathbf{A} . The eigenvalues of the matrix \mathbf{A} read $z_1 = \sqrt{x + x^2}$ and $z_2 = -\sqrt{x + x^2}$. It can be found that x = 0 is a second-order exceptional point of \mathbf{A} , and that x = -1 is another second-order exceptional point. The corresponding eigenvalue with the EPs is $z_0 = 0$ whatever x = 0 or x = -1. At the EP x = 0, the matrix $\mathbf{A}(0)$ is given by

$$\mathbf{A}(0) = \begin{pmatrix} 0 & 1 \\ 0 & 0 \end{pmatrix}, \tag{C2}$$

which has only one second-order Jordan block corresponding to its eigenvalue 0. In contrast, at non-EP the

matrix $\mathbf{A}(x)$ has two first-order Jordan block corresponding to z_1 and z_2 respectively.

Now, we will investigate the pseudospectrum of $\mathbf{A}(x)$, in which for simplicity, the 2-norm is used in Eq. (9). Given $\epsilon > 0$, one can analytically obtain the boundary of the ϵ -pseudospectrum $\sigma_{\epsilon}(\mathbf{A})$, which is given by the following equation associated with z:

$$\epsilon = s_{\min}(\mathbf{A} - z\mathbf{I}) = \frac{\sqrt{3x\bar{x} + 2z\bar{z} + 1 - \sqrt{\Delta}}}{\sqrt{2}}, \quad (C3)$$

where the expression of Δ is

$$\Delta = (\bar{x})^2 (5x^2 - 4x + 4z^2) + 2\bar{x}(6xz\bar{z} - 2x^2 + x + 2z^2) + 4x(x+1)(\bar{z})^2 + 4z\bar{z} + 1.$$
 (C4)

For the EP x=0, solving z associated with ϵ from Eq. (C3) and Eq. (C4), one arrives at

$$|z - z_0| = \sqrt{\epsilon(1 + \epsilon)}. \tag{C5}$$

Therefore, the ϵ -contours of $\sigma_{\epsilon}(\mathbf{A})$ are a group of concentric circles centered at the origin whose radius are $\sqrt{\epsilon(1+\epsilon)}$. Similarly, for another EP x=-1, the ϵ -contours are also a group of concentric circles centered at the origin with radius $\sqrt{\epsilon(2+\epsilon)}$. It is obvious that in both cases $|z-z_0| \propto \epsilon^{1/2}$ when $\epsilon \to 0$. Thus, q=2 and is just the order of the largest Jordan block of $\mathbf{A}(0)$.

For the case that x is real with $x \neq 0$, there are two branches of equations of ϵ -contour in polar coordinates, which are respectively

$$\rho_{+} = \sqrt{x^{2} \cos(2\theta) + x \cos(2\theta) + \epsilon^{2} + \sqrt{\Delta_{1}}}, \text{ (C6)}$$

$$\rho_{-} = \sqrt{x^{2} \cos(2\theta) + x \cos(2\theta) + \epsilon^{2} - \sqrt{\Delta_{1}}}, \text{ (C7)}$$

$$\Delta_{1} = \left(x^{2} \cos(2\theta) + x \cos(2\theta) + \epsilon^{2}\right)^{2}$$

$$-(x^{4} + 2x^{3} - 3x^{2}\epsilon^{2} + x^{2} + \epsilon^{4} - \epsilon^{2}). \text{ (C8)}$$

Then, we consider the process that x varies within (-1,1). When -1 < x < 0, z_1 and z_2 are pure imaginary. As x increases to 0, the distance between the two eigenvalues increases first and then decreases, and the two eigenvalues coincide at x = 0. When 0 < x < 1, as x increases from 0, the two eigenvalues bifurcates from 0 to

the real axis. In both cases -1 < x < 0 and 0 < x < 1, there is a critical

$$\epsilon_c = \left| \frac{1}{2} (\sqrt{5x^2 + 2x + 1} + x - 1) \right|,$$
 (C9)

such that for $\epsilon < \epsilon_c$ the ϵ -contour is a set of closed curves around the two eigenvalues respectively, and for $\epsilon > \epsilon_c$ the contour is a curve that surrounds both two eigenvalues. This is caused by the fact that when $\epsilon < \epsilon_c$ the two branches ρ_+ and ρ_- are all real and positive, and they together form a set of closed curves that surrounds the two eigenvalue respectively, but when $\epsilon < \epsilon_c$ only ρ_+ is real and it forms a curve that surrounds the two eigenvalues. In order to confirm the above process, we plot $-\ln(\epsilon)$ together with some of the ρ_\pm curves in Fig. 6.

Now, we consider the scaling behavior of ϵ -pseudospectrum contours for non-EP case. From Eq. (C6) and Eq. (C7), we can find that for x>0 the ϵ -contour surround z_1 satisfies

$$|z - z_1| = \sqrt{\rho^2 + |z_1|^2 - 2\rho|z_1|\cos(\theta)}$$

= $f(\theta, x)\epsilon + \mathcal{O}(\epsilon^2)$, (C10)

where $f(\theta, x)$ is a function of θ and x, and thus $|z-z_1| \propto \epsilon$ as $\epsilon \to 0$. For the contour surround z_2 and the case x < 0, or generally when the central eigenvalue is simple, we can similarly find that the radius of the ϵ -contour proportional to ϵ , which is consistent with the non-EP behavior mentioned in Sec. III.

Appendix D: Horizontal and vertical sample points of pseudospectra for EP and non-EP configurations

To quantitatively analyze the scaling behaviors of ϵ -pseudospectrum contours, we examine horizontal and vertical sample points of the pseudospectra shown in Fig. 5. Specifically, these sample points come from the left of and below the central spectrum (the fundamental mode for non-EP cases, and the coalesced mode for EP cases).

We depict $-\ln(\epsilon)$ against $-\ln(|\omega - \omega_0|)$ for non-EP configuration in Fig. 7, while $-\ln(|\omega - \omega_{\star}|)$ for EP configuration in Fig. 8, where $\omega_{\star} = (\omega_{+} + \omega_{-})/2$ provides an estimate of the coincident spectrum at the EP. The slope of these logarithmic plots directly reveals the scaling exponent: slopes approaching 1 indicate linear ϵ scaling characteristic of non-EP cases, while slopes approaching 2 confirm the $\epsilon^{1/2}$ scaling at EPs predicted by our theoretical analysis.

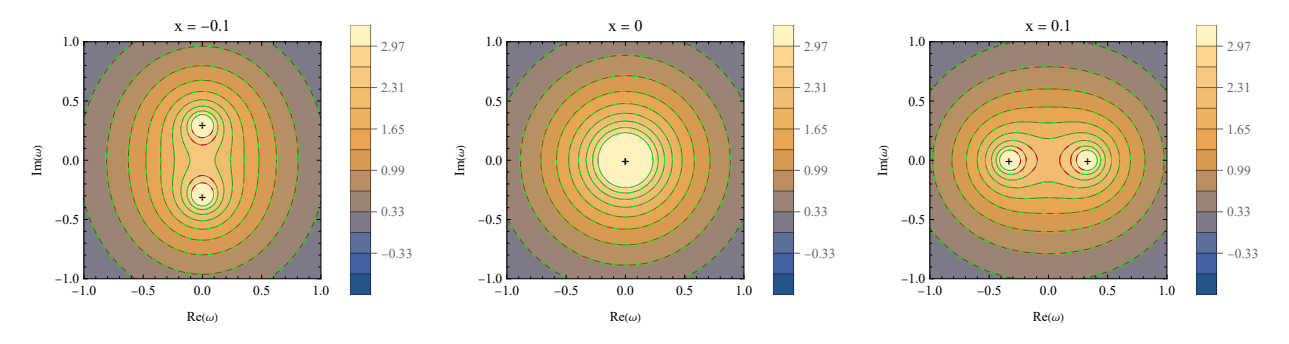


FIG. 6. Pseudospectrum for the toy model at x = -0.1, 0, 1. The dashed green lines are some of the ρ_+ branch curves and the dashed red lines are some of the ρ_- branch curves. The symbols + mark the eigenvalues of $\mathbf{A}(x)$ in (C1).

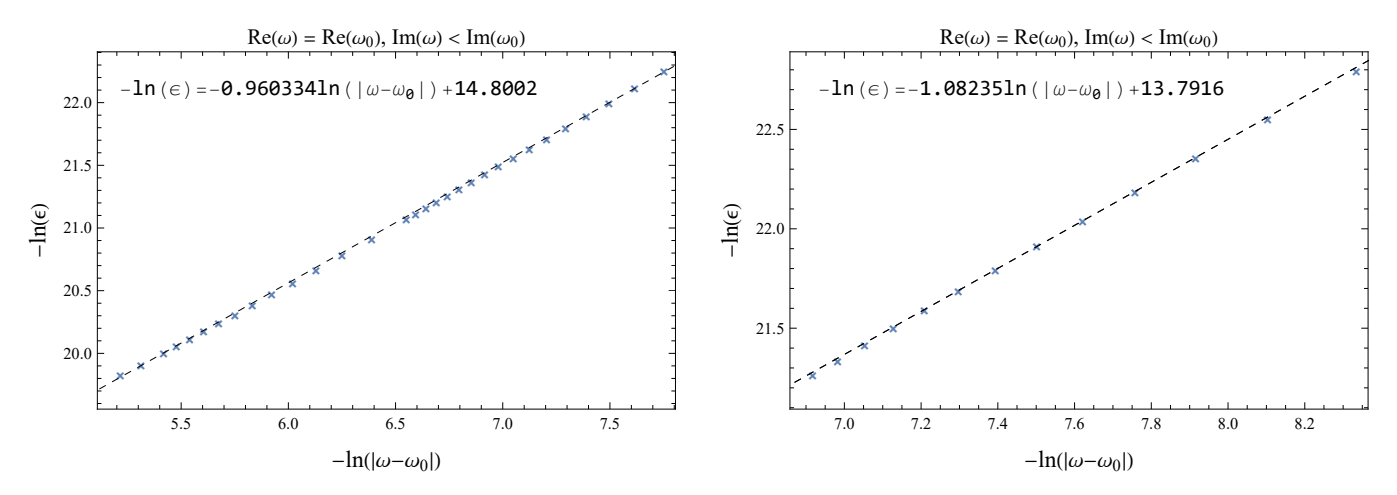


FIG. 7. Horizontal (left) and vertical (right) sample points of pseudospectrum at $\varepsilon = 0.005$, d = 15, $2\sigma_0^2 = 1$ (non-EP case). The symbols \times denote pseudospectrum data points, while the dashed lines show linear fits. The slope, approximately 1, confirms the ϵ scaling for non-EP case.

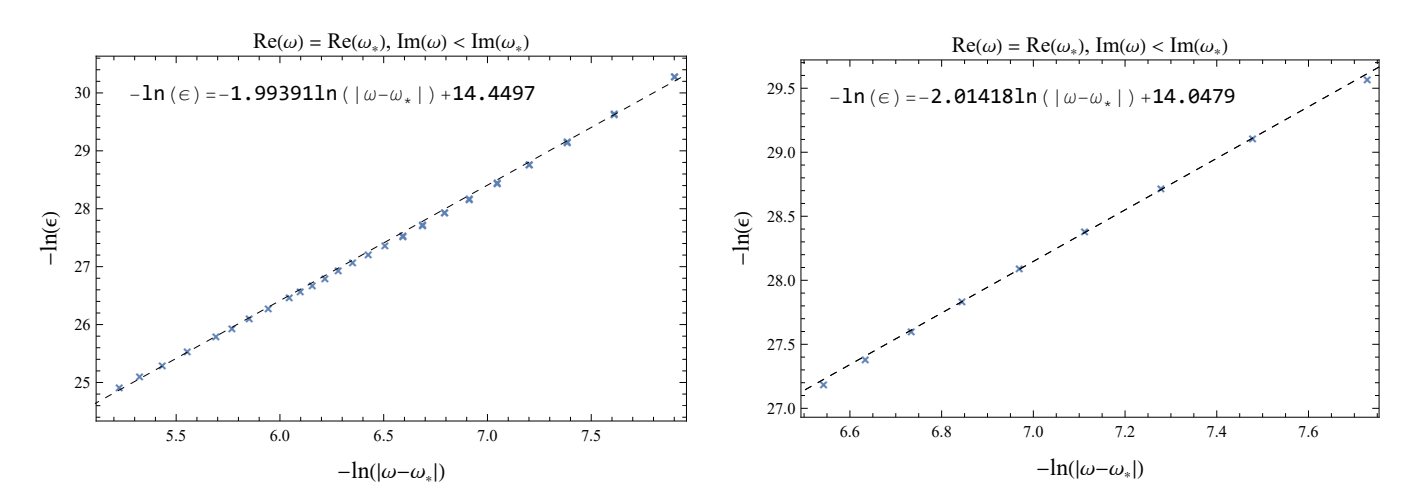


FIG. 8. Horizontal (left) and vertical (right) sample points of pseudospectrum at the exceptional point $\varepsilon = 0.005083$, d = 15.6976, $2\sigma_0^2 = 1$ (EP case). The symbols \times denote pseudospectrum data points, while the dashed lines show linear fits. The slope, approximately 2, confirms the $\epsilon^{1/2}$ scaling predicted by our theoretical analysis for second-order EPs.